EXPERIMENTAL INVESTIGATION OF AEROTHERMAL PROBLEMS ASSOCIATED WITH HYPERSONIC FLIGHT OF HST

K. HOZUMI, S. NOMURA
National Aerospace Laboratory
Chofu, Tokyo
Y. AIHARA, E. MORISHITA and T. OKUNUKI
University of Tokyo
Bunkyouku, Tokyo

Abstract

In order to investigate the aerothermal problems associated with HST with a sharp-edged wing, aerodynamic heating tests on the previously proposed hypersonic transport configurations were conducted using the NAL 50 cm hypersonic blow-down tunnel at the estimated cruse condition of M = 5. An investigation was also conducted at Mach numbers of 5.05, 7.1 and 12.0 to obtain aerodynamic heat transfer data on wing leading edge, especially in the peak heating regions by using flat plate models. The thermographic data over the wing and fuselage were accurately obtained by infrared(IR) scanning camera observation. Detailed local aerodynamic heat transfer distribution on a HST model was obtained from the IR thermographic data. The effect of the angle of attack and wing sweep angles on aerodynamic heating in the leading-edge region and on the boundary layer transition on the compression surface of the model were also examined. The results of the present studies give valuable heat transfer data and some insight into designing HSTs with configuration with sharp-leading edges and high L/D aerodynamic characteristics.

1. Introduction

Many authors have conducted numerous studies on feasibility of Hypersonic Transport for many years in many countries[3-4]. Experimental studies on the future of hypersonic transport aimed at maximizing the lift and minimizing the drag have been conducted by the present authors[1,2]. The study results indicate that hypersonic aircraft cruising beween Mach 5 to 7 are able to carry large payloads over long ranges and may be economically feasible as a proposed long-range transport.

In developing such vehicles, the accurate estimation of the performance of the HST depends to a large extent on how accurately heat transfer can be estimated at hypersonic speeds. According to these estimates, heat load optimizations would be of great importance, as the vehicle is expected to encounter extremly high heating rates.

During cruise, the HST should stand relatively lower but long-term constant heating levels compared to the re-entry vehicle and the space plane. However, in order to operate efficiently in cruise, design of vehicles having high lift over drag (L/D) ratio, that is, high L/D and low drag performance, are required. Low angle attack flight and sharp nose and wing leading edges configurations are essential to meet such a requirement[1,2]. Consequently, the HST may receive severe aerodynamic fuselage heating because of their flight at relatively low angle of attacks. Furthermore, for a vehicle with sharp leading edges, the aerodynamic heating of wings in hypersonic flight is most severe at the leading edges.

The purpose of the present study is to investigate the aerothermal problems associated with sharp-edged wing HSTs. To obtain heat-transfer data of these vehicles, especially in the peak heating regions, an experimental investigation of aerodynamic heating on the previously proposed hypersonic transport configurations type IV was conducted at the estimated cruise conditions of M = 5 at the NAL 50c hypersonic blow-down tunnel. Heat transfer measurement tests to obtain heat transfer data of peak aerodynamic heating on the wing leading edge were also conducted at Mach numbers of 5.05, 7.1 and 12.0 by using flat plate models.

2. Apparatus and Model Description

2.1 The Test Facility and Test Conditions

The tests were conducted in the NAL 50cm hypersonic wind tunnel at Mach numbers of 5.05, 7.1, and 12.0 and at angles of attack between -10° and 10° and side-slip angle of 0°. The Reynolds number range tested was approximately 3.5 to 9 million per meter. Further details of the tunnel and its operating characteristics are given in Reference 5.

The cruising type HST model IV [2] was set in the hypersonic wind tunnel of NAL at Mach number of 5.05, and the aerothermodynamic heating test was conducted at angles of attack of 0° and 10°. The details of the experimental conditions are shown in Table 1. The variable sweep test of flat plate was conducted at Mach number of 5.05, 7.10 and 12.0 to investigate the heating rate of the leading-edge more precisely. The test

conditions for sharp flat plate models are shown in Table 2.

2.2 Models

The Stycast model of the cruising type HST IV used in the present test is shown in Fig.1. The model has a strake of 83° leading edge sweep on the main wing. The wing has a clipped delta design with a 70° leading edge sweep and a 10° trailing edge sweep. The wings have flat-sided wedges with rounded leading edges. The leading edge radius of the wing is approximately 0.1 mm at the wing root and varies from root to tip.

The flat plate models of ground finished machinable ceramics (Macol type p) have 10.0 mm thick for the flat parallel part. The configuration of the flat plate models is shown in Fig.2. Two different leading-edge cross-sections with 0.3mm thick at the edge (type I leading edge) and 0.75mm thick (type II leading edge) were tested at Mach number of 5.05 and 12.0, and 7.1, respectively. The leading-edge sweep of this model could be varied in axis near the center of the model; thus, the model have the five different wing sweep angle of 27°, 40°, 55°, 70°, and 83°.

3. Test Procedure and Instrumentation

3.1 Heat Transfer Measurement Technique

Thermal mapping of the heating patterns that convective heating induced on wind tunnel models was obtained by using the commercially available infrared (IR) scanning system. Two IR video system of 4 and 8 bit temperature resolution with 256 X 100 pixels and 30 frame/sec and 100 frame/sec scanning speed, respectively, were used. The IR imaging system was positioned inside the test section, above and below the main free-jet, to obtain leeward and windward data simultaneously.

The models were sting-supported in the tunnel test section and were injected in a few tenths of a second at a pre-set angle of attack by mean of high speed ejection system with an air cylinder. To determine the model injection time and initial time of heating (t=0), 3 trigger pulses at positioned at the injection start, nozzle boundary layer edge, and center of wind tunnel were used.

The data were recorded on digital form cassette tape. Processing the data from tape and the reduction of aerodynamic heating were done in off-line mode, by transferring the digitized temperature data of the IR image record to the NAL computing system.

3.2 Heat Transfer Data Reduction

Thermal mapping data are especially important to obtain complex model's heat transfer data. The aerothermodynamic heat transfer distributions of the cruising HST model were obtained by the Jones-Hunt[6] method by using time history of surface temperature on the model from the IR image data.

Factor affecting the data accuracy are carefully examined. The model emittance was experimentally determined by uniformly heating to a known temperature, and measuring the IR images's radiant emittance. The emissivity of Stycast and Macol Type P was measured to be 0.95 and 0.74, respectively, for the temperature range of the present test.

Determing model outline edges are very important for data analysis. They are carefully determined from the initial image outline of models just before the start of test. Using this model outline, a false high temperature illumination region around the model's edge was removed.

Difference in initial temperature significantly affects the accuracy of data. The model initial temperature was measured from the thermocouple output on the model and initial image of IR camera by setting camera temperature measurement range at high sensitivity temperature resolutions. The model's initial temperature was not controlled.

4. Results and Discussion

4.1 Heat Transfer Experiment of Cruising Type HST Model IV

4.1.1 Overall Heat Transfer Characteristics

Angle of Attack of 0° The aerothermodynamic heat transfer distributions of the cruising HST model are shown in Figs.3a) and b). The Stanton number St_∞ is calculated based on the uniform stream conditions and the adiabatic wall temperature of the flat plate laminar boundary layer.

Fig3.a) shows the heat transfer of the windward side at t=5.37 seconds, where t denotes the time after the model is set in the hypersonic wind tunnel. It is clearly observed that the nose and the downstream leading edge of the double delta wing are heated intensively. The downstream leading edge is a supersonic one. The Stanton number is in the order of 10^{-3} in these regions. The angle of attack of the windward side of the double delta wing is zero when that of the HST model is zero. The upstream leading edge of the double delta wing, which is subsonic one, is not heated so much due to the higher swept angle.

The shape of the nose is not clearly visible because the radiation fromo the compressed air, probably due to the carbon dioxide and water vapor, is detected by the infrared camera. The same phenomenon is observed in the downstream leading edge of the double delta wing. The temperature increases gradually in these regions, and these do not

necessarily correspond to the actual body location. The model edge is probably situated in a position just before the highest heat transfer is reached. The view of the 4-bit infrared camera set on the windward side is divided by 128 and 100 in the x- and y-directions respectively, as shown in Table 1. The spatial resolution is about 2mm x 2.2mm in the x- and y-directions respectively, and therefore there appears the ambiguity of this order in the body configuration.

Fig.3b) shows the leeward side heat transfer obtained from the data at t=6.50 seconds. The 8-bit infrared camera on this side has 256 x 100 divisions in the x- and y-directions respectively. The spatial resolution is about 1mm x 1.7mm in the x- and y-directions respectively. The nose was out of sight due to the spatial restriction of the hypersonic wind tunnel, and the highest heat transfer region is not included perfectly in the figure. The severe heat transfer in the downstream leading edge of the double delta wing, however, is clearly visible as on the windward side. The Stanton number is of the same order as on the windward side, although a slight compression occurs in the leeward downstream leading edge of the double delta wing because the wing surface has a small inclination at angle of attack of 0° . The heat transfer in the leading edge region also increases gradually, due to the radiation from the compressed shock region. The gradual increase in heat transfer does not mean that the leading edge has a lower Stanton number.

(The upper wing tip is about to brake in Fig.3b), and a higher heat transfer is observed in the region because the surface is deformed.)

The heat transfer is not so high in the fuselage region of the leeward side in spite of its shape.

Angle of Attack of 10° Fig.4 a) shows the Stanton number distributions on the windward side at t=6.27 seconds. The heat transfer pattern is similar to that at angle of attack of 0° . The nose and the downstream leading edge region of the double delta wing are exposed to higher heating than at angle of attack of 0° , due to compression. The radiation from the compressed shock region makes the body configuration unclear. The order of the Stanton number is also 10^{-3} in this case. The 8-bit infrared camera was employed for this side.

Fig.4b) shows the heat transfer distribution of the leeward side at t=5.28 seconds. The infrared camera is 4-bit on this side. This side corresponds to the expansion region, and a slightly lower Stanton number is obtained. The nose and the downstream leading edge are also exposed to higher a heating rate, and the order of the Stanton number is 10^{-3}.

4.1.2 Heat Transfer in Cross Section

Angle of Attack of 0° Fig.5a) shows the heat transfer distribution in cross sections along the body axis of the HST model. The bold lines correspond to the windward surface and the thin lines to the leeward surface.

The upstream leading edge of the double delta wing has a higher heat transfer at x/L=0.313, where x is the distance from the nose and L (=320mm) is the body characteristic length. The fuselage is also heated on the leeward side, and three peaks are observed.

Both sides have similar heat transfer distributions at x/L=0.594, and the leading edge is heated.

At x/L=0.750, the downstream leading edge of the double delta wing is exposed to a higher heat transfer. Although the leeward side of the leading edge has a small inclination against the uniform stream direction, the Stanton number is about the same as that of the windward side. The central region of the windward side has a flat heat transfer distribution because of the shape of the windward surface. Both sides of the fuselage have a slightly higher heat transfer on the leeward side. The flow in the region is in the downstream of the junction of the double delta wing, which could affect the heat transfer. The asymmetry of the heat transfer distribution might be attributed to the break of the wing tip (see Fig.3b) and Fig.5b) or a very small roll angle.

The heat transfer distribution at x/L=0.844 is similar to that at x/L=0.75. There is a small heat transfer peak in the central region of the windward side, although the surface inclination is zero against the uniform flow at this location. The reason for the small peak is, therefore, not quite clear. An asymmetry in heat transfer is also observed, as at x/L=0.75. The heat transfer on the windward side has a higher peak than that on the leeward side, although there is no surface inclination of the windward surface. The 4-bit camera was employed for the windward surface. The temperature sensitivity is worse than on the leeward side, as shown in Table 1. This is surely one of the reasons why the windward surface shows slightly higher heat transfer distributions.

A higher heat transfer is observed at x/L=0.844 than at x/L=0.750. This is considered to be the effect of leading edge thickness. The leading edge becomes thinner downstream, and the temperature increases rapidly. The Jones-Hunt method is based on the 1-dimensional heat conduction of semi-infinite thickness and ,therefore, could give an apparently higher Stanton number at the leading edge. The heat conduction effect is discussed later in the present paper.

At x/L=0.891, the heat transfer distribution is similar to that at x/L=0.750. (The higher peak on the right hand side is due to the brake of the wing tip.)

Angle of Attack of 10° Fig.5b) shows the cross-sectional heat transfer distribution. The leading edge heat transfer peak disappears on the leeward

side due to expansion at x/L=0.313. A peak is observed on the fuselage top because the fuselage has a positive angle of attack even at this attitude. The leading edge has a higher Stanton number on the windward side.

At x/L=0.594, the leading edge peak appears even on the leeward side. The heat transfer distribution is rather flat in this cross section.

The windward heat transfer is naturally higher than the leeward one at x/L=0.750. Two small heat transfer peaks are observed on top of the fuselage on the leeward side, which could be an effect of flow characteristics such as reattachment of the flow, as stated later. The windward heat transfer distribution shows a complicated pattern, which is also caused by the 3-dimensional nature of the flow. The infrared photograph of the same surface exhibits that there are low temperature lines along the flow direction in regular pitch and there seem to be longitudinal vortices due to the inclination of the body surface.

4.1.3 Comparison with Pressure Distribution

Angle of Attack of 0° Although the pressure distributions are not shown explicitly in this paper, Newtonian pressure distributions were obtained from the geometry of the model and compared to the experiment[2]. The result showed that the measured pressure distribution was similar to the Newtonian flow pressure coefficient C_p. The Newtonian pressure distribution is therefore used to discuss relations between the heat transfer and

The central heat transfer peak on the leeward side corresponds to high C_p, i.e., the compression due to flow deflection at x/L=0.313.

At x/L=0.75, the windward side C_p is zero from the Newtonian flow theory, and the heat transfer in the central region is also very flat except at the leading edge. Two small heat transfer peaks are visible in the leeward central region, and C_p is correspondingly positive. Although C_p also has a peak on the fuselage top, the heat transfer distribution has a valley in the region.

The Newtonian C_p and the heat transfer distributions are fairly flat at a larger x/L , except the heat transfer peak at the leading edge.

Angle of Attack of 10° The Newtonian C_p on the leeward side becomes mostly negative, and the heat transfer distribution is thereby lowered. At x/L=0.313, the fuselage top still has a positive angle of attack and therefore experiences a higher heat transfer rate.

4.1.4 Comparison with Flow Patterns

The surface oil-dot flow visualization result is available at M=7 and angle of attack of 7° [2]. The windward surface flow pattern is almost 2-dimensional except at the wing-body junction, where a 3-dimensional flow is observed. The corresponding heat transfer distribution at x/L=0.750 exhibits some irregularities in this region, although in the present experiment M=5.05 and the angle of attack is 10 degrees. The waviness in the heat transfer distribution could also be caused by longitudinal vortices in the present experiment, as stated above. (The oil-dot flow visualization of the windward surface in reference 2 does not show the vortices explicitly.)

The leeward flow pattern in reference 2 is more complicated than the windward side one. The surface streamlines go outward in the upstream region of the double delta wing and the fuselage. This is caused by the leading edge vortices. The surface streamlines on the downstream part of the double delta wing go inward to match the pressure distributions at the leading edge, separate near the body, and then seem to reattach on the fuselage sides. In the present experiment, the lower heat transfer region between the fuselage side and the wing leading edge at x/L=0.75 might correspond to this region. The two small heat transfer peaks on the fuselage sides could correspond to the flow reattachment region.

4.1.5 Heat Transfer Correction at Leading Edge

The present HST model has a sharp leading edge. The heat conduction effect should be corrected when the Jones-Hunt method is applied to this shape. The method gives an apparently higher Stanton number due to the heat conduction effect from both sides of the leading edge.

The temperature distributions of the downstream leading edge of the double delta wing in the present experiment seem to be almost 2-dimensional in the sense that the temperature gradient is effectively normal to the leading edge. The specific wing cross section normal to the leading edge can be treated as 2-dimensional. The heat transfer/conduction problem in this section can be treated by the quasi 1-dimensional method and/or 2-dimensional method.

Let s [= x*cos(Λ)] be the coordinate normal to the wing leading edge (see Fig.6). The heat transfer along s might be assumed to be proportional to $[\cos(\Lambda)]^n/\mathrm{sqrt}[s]$, while the coefficients are kept the same as the laminar boundary layer solution. Where Lamd is swept angle. The power n=0.5 is assumed here to match the experimental transient temperature rise.

The assumed heat transfer distributions are shown by lines in Figs.6a) and b) for angle of attack of 0° . Figs.6a) and b) show the windward and leeward sides respectively. The reference temperature method[7] is employed to get the above mentioned approximate heat transfer. The transient temperature rise is calculated by using the present experimental conditions for angle of attack of 0° .

The Jones-Hunt method can be applied to

the calculated result to obtain the Stanton number, shown in Figs. 6a) and b) by symbols o and +. The Jones-Hunt apparent Stanton number is definitely higher than the assumed one (and corresponding real one).

The experimental Stanton number at x/L=0.75 is projected on s and is shown in Figs.7a) and b) by the triangle and x symbols. Although the experimental values are not in exactly the same location as that of the calculation, the nearly 2-dimensional temperature distribution at the leading edge may validate this comparison. The comparison between the numerical analysis and the experiment, both obtained by the Jones-Hunt method, is fairly satisfactory, should it be mentioned the analysis is a semi-empirical one. The leading edge position is not exactly known in the experimental data, and therefore the data location is adjusted in Figs.7a) and b).

The Jones-Hunt method is shown to give higher values at the thin leading edge, as in Fig.5. The apparent Stanton number is affected not only by the configuration, but also by the model material characteristics.

A method can be proposed to avoid the heat conduction effect in such an experiment. The measured surface transient temperature is used as a boundary condition and the transient heat conduction equation of the model is solved numerically. The temperature gradient is then obtained on the model surface at each time step, and thereby the corresponding heat flux and the Stanton number can be obtained.

The method is applied to the numerical experiment mentioned above, and the Stanton number obtained by this particular method is shown by symbol * on the assumed Stanton number distribution lines in Figs.7a) and b). The agreement is quite satisfactory. The above method is also readily applicable to the present and other experiments, by employing the experimental temperature, and assures a more exact Stanton number at locations where heat conduction matters.

4.2 Heat Transfer Measurements on Flat Plate

To investigate the aerodynamic heating of the wing leading-edge more precisely, heat transfer measurements of flat plate were conducted.

4.2.1 Result of Unswept Flat Plate at α=0°

Examples of the centerline heat-transfer distribution at Mach number of 7.1 and at t=0.1, 3 and 5 sec are presented in Fig.8 in the form of Stanton number St_∞ based on free stream conditions. Heat-transfer rate calculations on flat plate based on laminar boundary layer theory[8] and strong-interaction theory[9] are also plotted for comparison.

At α =0°, the measured Stanton numbers on the centerline were much larger than the corresponding calculated two-dimensional laminar flat plate value at the leading-edge region (x ≦20mm). The value of the St_∞ decrease rapidly as distance increases from the leading-edge x. The slope of the decrease is steeper than the $Reinf^{-1/2}$ variation of the theory. In the down stream region sufficiently far from the leading-edge (x ≧ 30 mm), the magnitude of the measured value is lower than the laminar boundary layer theory estimation and rather close to the magnitude of the strong-interaction theory estimation . (In the region of x ≧ 2-3 cm in Fig.8, the model surface temperature did not reach to the enough high sensing range of temperature of IR camera and was used for the present analysis.)

The some reason for the great difference between the measured and the estimated values at the leading-edges might be due to the high viscous-interaction-induced pressure near the leading edge region from which feeds low-energy boundary-layer fluid. In the present tests, for tests at a Mach number of 12 this interaction effects are expected as strong interaction parameter χ =O(1) at leading-edge region. But at Mach numbers of 5 and 7 , the effect of viscous interaction is not as large (χ ≦ O(1)). Nevertheless, the measured curve along x approaches the interaction theory for all cases tested at Mach number of 5.05, 7.1, and 12.

Another reason for this discrepancy is, as already studied in previous section, the effect of heating the back surface of the model. At the leading edge region, the assumption of one-dimensional semi-infinite heat conduction for the present Jones-Hunt method may be violated shortiy after the start of heating. The estimated influenced region are shown in Fig.8. The relation between maximum test time $t_{d,1}$ and the depth of heat penetration 1 and thermal diffusivity α is

$$t_d = 0.2*1^2/\alpha \qquad (1)$$

Twice of the penetration depth was used for plate thickness d to determine the boundary of violation of the one-dimensional assumption by heating both side. Figs.8 show that at t=5 and 3 sec, violation of the assumption at the leading-edge region was expected but at t = 0.1 sec, thickness of the leading-edge d is within the depth of heat penetration 1.

The reason for the high heating rates measured at the leading-edge in the present tests is unknown presently, but it should notes that the amount of heating at the leading edge region is evidently higher than the existing theoretical values and that there is some consistency to the wing leading-edge heating of the HST configuration in section 4.1.

4.2.2 Effect of Mach Number and Angle of Attack for Unswept Flat Plate

The heat-transfer rate level for α = 10° based on free stream condition is greater than that for α = 0° at far enough down stream from the leading edge, and is near the laminar theoretical value based on flow conditions after the oblique shock. Higher heat transfer rates at the leading edge region are similar as the above mentioned α= 0° case.

In order to properly apply one dimensional semi-infinite heat conduction method assumption, the heat transfer coefficient at time t=0.1 sec is obtained by the Jones-Hunt Method and checked by the thin film data reduction technique[10] for the temperature history of pixel near the leading edge. Results obtained from this analysis of the effects of Mach numbers and angle of attack on this peak heating at the leading-edge region are shown in Fig.9.

Comparison with the magnitude of peak heating between α = 0° and α = 10° showed that at the leading edge, the heat transfer rate of α = 0° is higher than that at α = 10°. Fig.9 also shows that as Mach number increases the heat transfer of the leading edge region increases.

The trends are presumably due to the strong viscous interaction at the leading edge region at α = 0°. At Λ = 10°, there might be suppression for the interaction due to shock loss effect from oblique shock at the leading edge. Further investigation will be necessary to clarify these results.

4.2.3 Effect of the Sweep Angle on Heat Transfer Data

Evaluation of the effect of the sweep angle on wing leading edge heat transfer is important for a HST design. There are many slab delta wings investigation[11]. However, little data other than CFD works results[12] is available for sharp delta wings at the near range of Reynolds number and Mach number to the present tests.

The result of the present peak heating tests with the sweep angle effect are shown in Fig.10. The present data shows rapid heating rate decrease as the sweep angle Λ increases. Peak heating at α = 0° decreases rapidly near low sweep angles and changes less at higher Λ. The peak heating at α = 10° showed relatively gradual decrease from the value at Λ = 0° which is lower than that at α = 0°.

In the previous studies[2,13], the difference of oil flow pattern on the windward face of a delta wing and inviscid flow direction at boundary layer edge. The angle of attack dependancy of these three-dimensional flow near the leading edge or a three-dimensional cross flow may be the cause of the differnce of effects of sweep angle between α = 0° and 10° case in the present tests.

4.2.4 Transition Observation on Swept and Unswept Flat Plate Surfaces

The influence of such factors as Mach number, leading-edge sweep, and bluntness on transition are of considerable importance. Characteristic features of the present test observation of the boundary layer transition are shown in Figs.11. The increase of heating resulting from a turbulent wedge is clearly seen.

Two types of leading edges are used in the present tests as shown in figure 2. Type I leading edge tested at Mach numbers of 5.05 and 12.0 have very thin 0.3 mm thick leading edge. The edges are slightly contaminated after several tests. For Mach number of 7.1 tests, slightly blunter 0.75mm thick edges are used to avoid this. The IR image photo copy showed leading-edge effect from this difference. The difference of the transition onset line is shown in Figs.11 a),b),c). Turbulent wedges or the irregular onset of transition fronts are observed for type I leading edge case at M = 5.05. Type II leading-edges tested at M =7.10 show a uniform onset of transition parallel to the leading edge are observed. For the test at α = 10° and Λ= 55°, earlier transition onsets at the same flow condition and sweep angle. This difference apparently comes from the difference between contaminated and non-contaminated leading edge. These observations show that attachment line instability caused by by contamination[15] is one of the dominant mechanism for sharp (slightly blunt)leading edges.

The present tests observes the well established trend that at supersonic Mach numbers, increases in sweep reduce the transition Reynolds number as expected. The mechanisms responsible for transition on swept surfaces have been suggested[14,15] as crossflow instability and attachment line instability caused by contamination and instability. Leading-edge shock wave effects hvae been also considered[16]. Changes in local Reynolds number, due to shock strength, were analyzed to have considerably more effect on transition caused by Tollmein-Schrlichting instability than on that caused by crossflow instability.

The positions of onset of transition were measured from the surface thermographics of the present tests. The onset of transition was taken to be the position where the wall temperature begin to increase along the plate. Fig.12 shows change in transition Reynolds number with sweep angle is presented as the ratio between transition Reynolds numbers of unswept flat plate and swept flat plate. For case of Mach number of 7.1, flat plate transition Reynolds number at α = 0° and Λ = 0° are estimated from sharp cone transition Reynolds number at the same flow condition as no corresponding data of flat plate transition Reynolds number was measured. The ratio of unit Reynolds number change due to the normal and oblique shock is also shown in Fig.12. Relatively good agreement with

this curve was shown in the present tests. These results for onset of transition of swept sharp flat plates tests shows that effect on unit Reynolds number caused by shock loss (shock loss effect)[15] are perhaphs mainly responsible to difference in transition Reynolds number between slightly blunt swept and unswept wing rather than the existence of crossflow instability associated with the blunt swept wing.

5. Conclusions

To investigate the feasibility of sharp leading edge HST configuration, heat transfer measurement tests at M = 5.05, 7.1 and 12.0 for the cruising type HST model and flat plate model were conducted.

The heat transfer distribution of the cruising type HST model at a Mach number of 5.05 showed that the nose and the leading edge heat transfer is most severe as expected. The magnitude of heat transfer on the leeward surface is almost same order as windward surface and also important in the design of cruising type HST.

In the present investigation, it became apparent that the sharp leading edge heat transfer could be overestimated when the heat conduction cannot be neglected. The heat conduction equation for the model was utilized to obtain an accurate heat transfer instead of the semi-infinite 1-dimensional heat conduction model.

In the present flat plate tests, the magnitude of heat transfer at the region near to the sharp leading edge was greater than the existing theoretical prediction. And results also showed great effects of the angle of attack and sweep angle on heat transfer in the leading edge region.

The IR thermographics observation clearly showed large effects of the angle of attack, sweep angle and leading edge roughness on transition.

The present tests data will give valuable data in developing a future hypersonic vehicle with sharp leading edges. However, it became apparent in the process of the present tests that the heating phenomena at the leading edge region is not fully understood at the present time. Further investigation of the leading-edge heating phenomena will be necessary to obtain the quantitative prediction of leading edge heating in design of HST.

Acknowledgment

The authors would like to express their heartfelt thanks to Mr. T. Tamura, research student, The University of Tokyo, who has helped them in data processing at NAL.

References

1) Y.Aihara, S.Nomura, A.Murakami and N.Sudani, "Configuration and Trajectory of Hypersonic Transport with Aerothermodynamic Control", ICAS-86-2.10.3 ,1986.
2) Y.Aihara, E.Morishita, T.Okunuki, S.Nomura and K.Hozumi, "Experimental Study on Drag Reduction of Hypersonic Transport Configuration" ICAS-90-3.10.1 1990.
3) Bushnell,D.W., "Hypersonic airplane aerodynamic technology" NASA SP-292, 1971.
4) Hankey, W.L., "Some design aspects of hypersonic vehicles", AGARD-LS-42, Lec. 8 , 1972.
5) Hiraki, I., et al., " Design and Construction of the 50 cm Hypersonic Wind Tunnel at National Aerospace Laboratory", NAL TR-116, Sep. 1966.
6) Jones, R.A. and Hunt,J.L, "Use of Fusible Temperature Indicators for Obtaining Quantitative Aerodynamic Heat-Transfer Data", NASA TR R-230, Feb., 1966.
7) Monaghan, R.J.," On the Behavior of Boundary Layers at Supersonic Speeds", 5th International Aeronautical Conference (Los Angels, Calif., June 20-23,1955), Inst.Aeron. Sci., Inc., 1955, pp277-315.
8) Van Driest, E.R., " Investigation of Laminar Boundary Layer in Compressive Fluids Using the Crocco Method", NACA Technical Note 2597, Jan. 1952.
9) Stolly, J.L., " Viscous Interaction Effects on Re-entry Aerothermodynamics: Theory and Experimental Results", Lec.10 in AGARD-LS-42 Vol.1, July 1972.
10) Cook,W.J.,and Felderman,E.J., " Reduction of Data from Thin-Film Heat-Transfer Gages: A Concise Numerical Technique", AIAA J. Vol.4, No.3, March 1966.
11) Bertram, M.H., and Everhart, P.E., "An Experimental Study of the Pressure and Heat-Transfer Distribution on a 70° Sweep Slab Delta Wing in Hypersonic Flow", NASA TR R-153, Dec. 1963.
12) Beauford Jr.,G.S., "Numerical Solution of the Supersonic and Hypersonic Viscous Flow around Thin Delta Wings", AIAA J., Vol.17, No.9, Sep. 1979.
13) Bertram, M.H., Feller, W.V., and Dunavant, J.C., "Flowfields, Pressure Distribution and Heat Transfer for Delta Wings at Hypersonic Speeds", NASA TMX-316, 1960.
14) Arnal,D.,"Laminar-Turbulent Transition Problems in Supersonic and Hypersonic Flows", in AGARD Report No.761 , June 1989.
16) Poll,D.I.A., "Development of intermittent turbulence on swept attachment line including the effects of compressibility", The Aeronautical Quarterly, Vol. XXXIV , 1983.
17) Jillie, D.W., and Hopkins, E.J., "Effects of Mach Number, Leading-Edge Bluntness, and Sweep on Boundary-Layer Transition on a Flat Plate", NASA TN D-1071, Sep. 1961.

Table 1 Experimental Conditions for HST model IV

Model	Run No.	α deg.	p_0 bar	T_0 K	M	Re 10^6/m	T_i K
HST IV	3341	0	8.23	580	5.05	8.1	286
HST IV	3342	10	8.22	575	5.05	8.2	291

Model	Run No.	side	Infrared Camera			
			divsions x x y	bit	Δ T deg.	Δ t/frame sec.
HST IV	3341	windward	128x100	4	9.0	~ 0.091
		leeward	256x100	8	0.41	~ 0.033
HST IV	3342	windward	256x100	8	0.63	~ 0.033
		leeward	128x100	4	5.0	~ 0.091

Symbols M : Machnumber, P_0:total temperature, Re : unit Reynolds number
T_i : model initial temperature, T_0 : total temperature
dt : time interval dT : temperature resolution
x,y,z: body axes system coordinates alpha: angle of attack

Table 2 Experimental Conditions for Flat Plate Model

M	P0 (bar)	T0 (°K)	Re/m($\times 10^{-7}$)	α (deg)	Λ (deg)
5.05	8.2	560 - 580	0.8 - 0.83	0 10	0, 27,40 55,70,83
7.10	29.8	760 -800	0.78 - 0.9	0 10	0, 40 55,70
12.0	88.6	1115	0.366 - 0.375	0	0 10

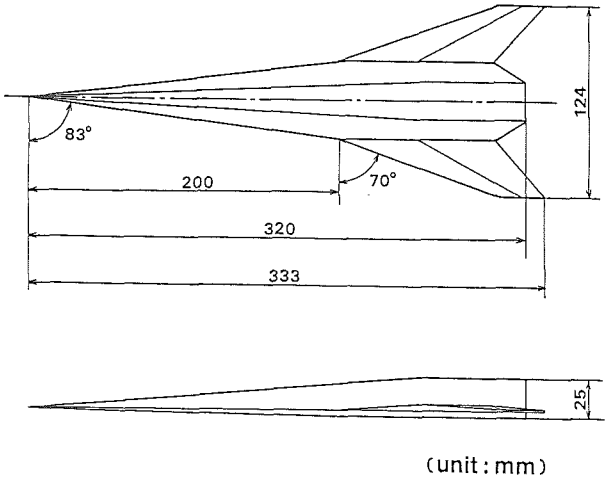

Fig.1 Wind tunnel model : HST type IV

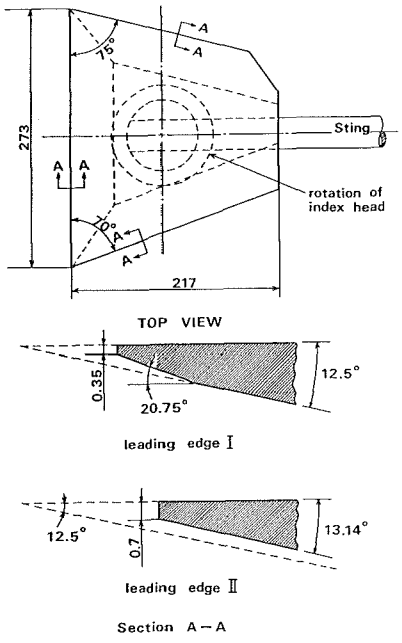

Fig.2 Wind tunnel model: Flat plate model

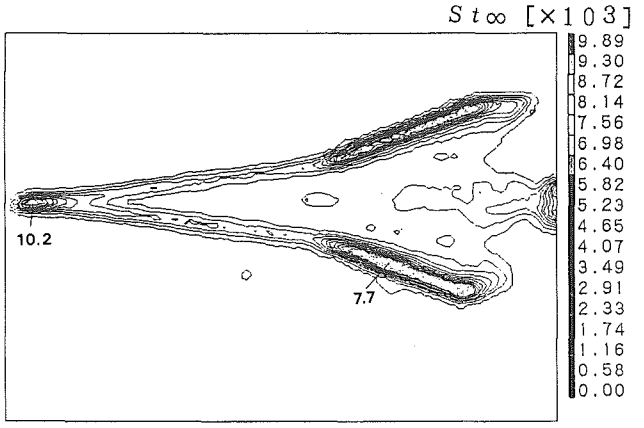

Fig.3a) Model HST Heat Transfer of Windward Side
[M=5.05 Angle of attack = 0 deg.]

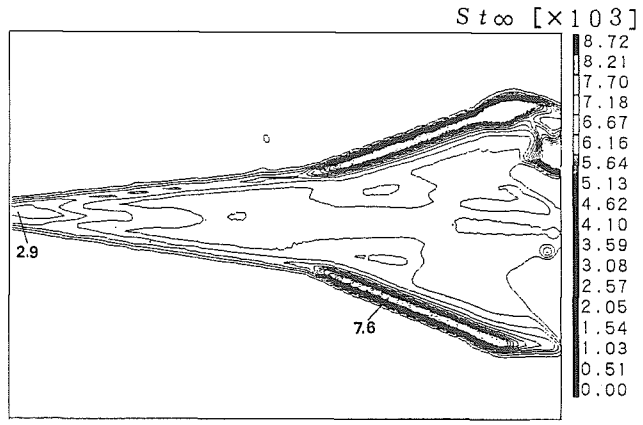

Fig.3b) Model HST Heat Transfer of Leeward Side
[M=5.05 Angle of attack = 0 deg.]

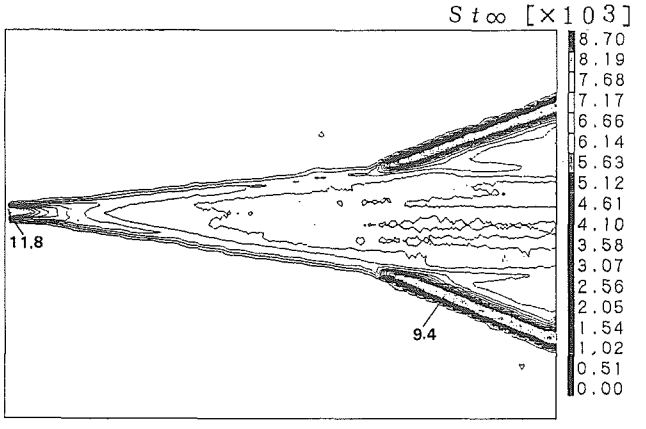

Fig.4a) Model HST Heat Transfer of Windward Side
[M=5.05 Angle of attack =10 deg.]

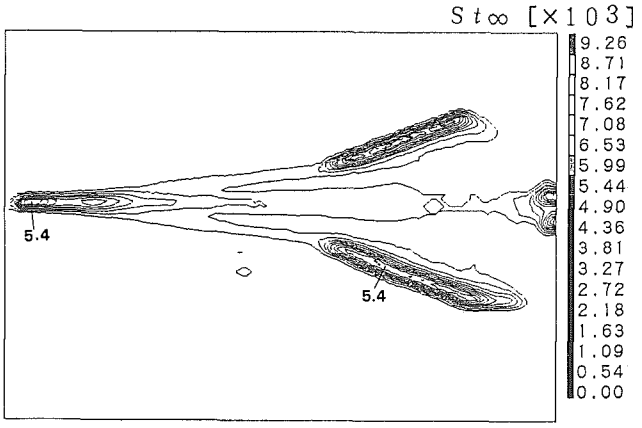

Fig.4b) Model HST Heat Transfer of Leeward Side
[M=5.05 Angle of attack =10 deg.]

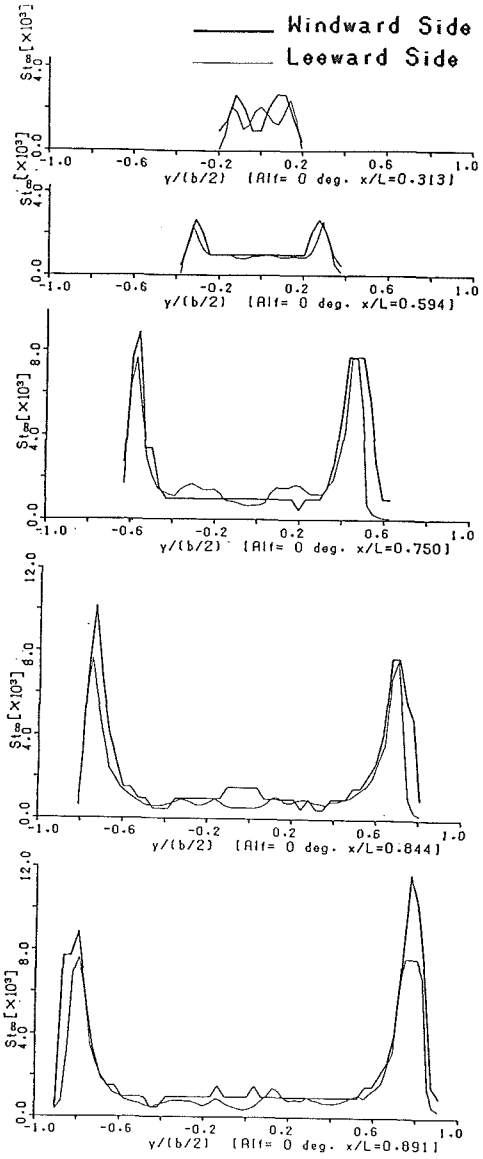

Fig.5a) Cross-sectional Heat Transfer Distribution
[M=5.05 Angle of attack = 0 deg.]

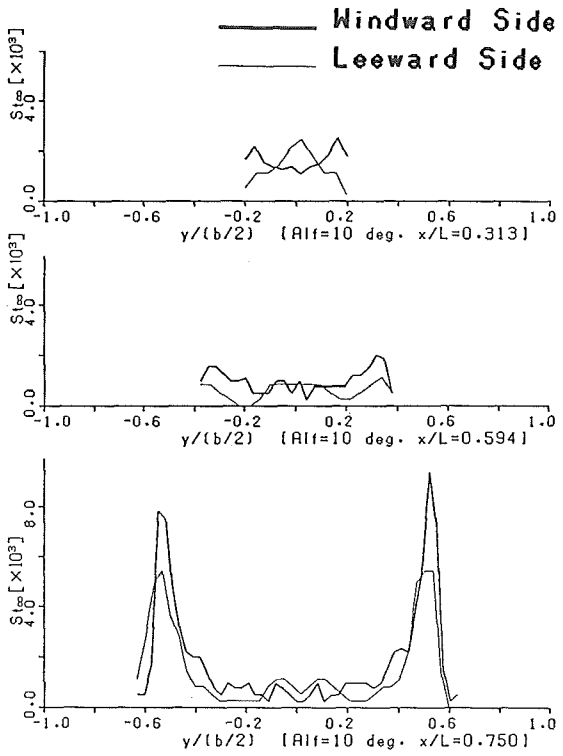

Fig.5b) Cross-sectional Heat Transfer Distribution
[M=5.05 Angle of Attack =10 deg.]

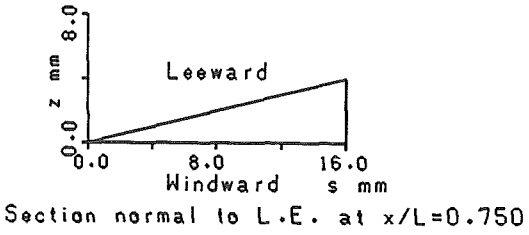

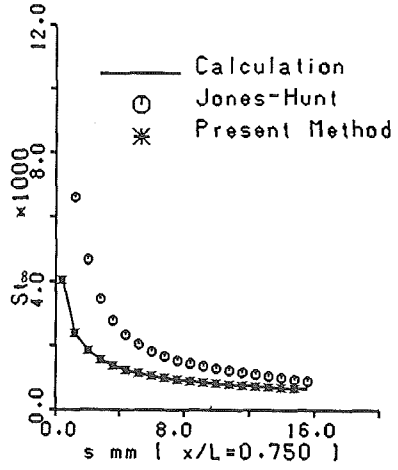

Fig.6a) Windward Heat Transfer at Leading Edge
[M=5.05 Angle of attack = 0 deg.]

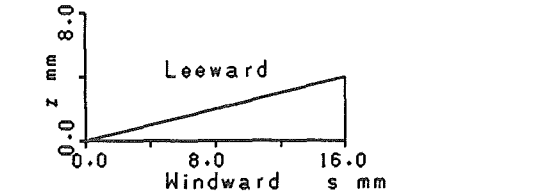

Section normal to L.E. at x/L=0.750

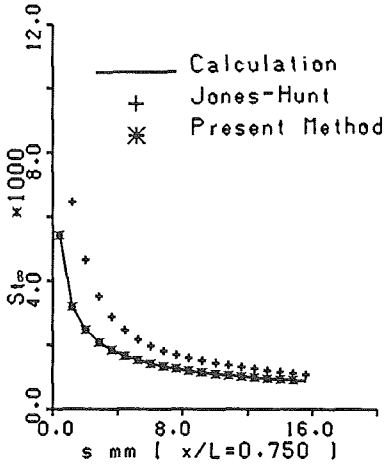

Fig.6b) Leeward Heat Transfer at Leading Edge
[M=5.05 Angle of attack = 0 deg.]

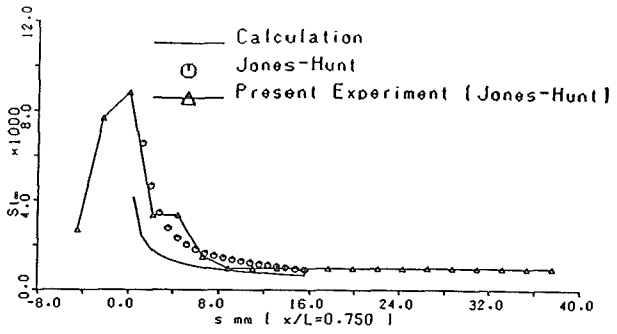

Fig.7a) Windward Heat Transfer at Leading Edge
[M=5.05 Angle of attack = 0 deg.]

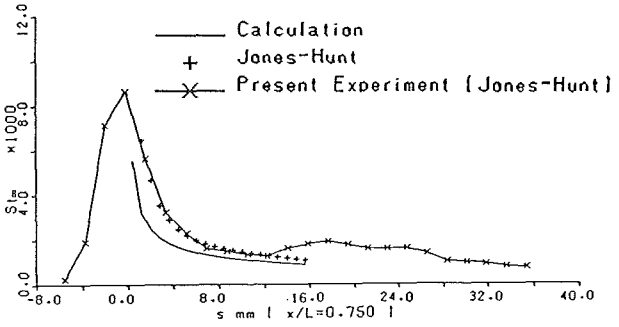

Fig.7b) Leeward Heat Transfer at Leading Edge
[M=5.05 Angle of attack = 0 deg.]

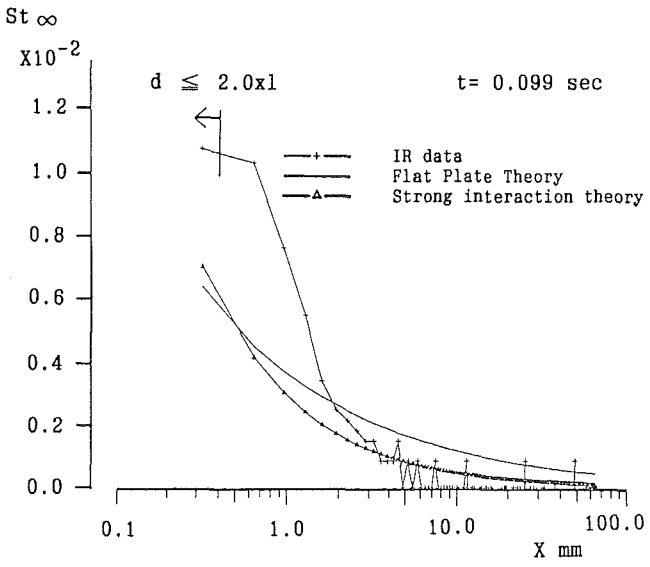

Fig.8a) Heat transfer distribution along centerline of flat plate
(M= 7.1, α = 0°, t= 0.099 sec)

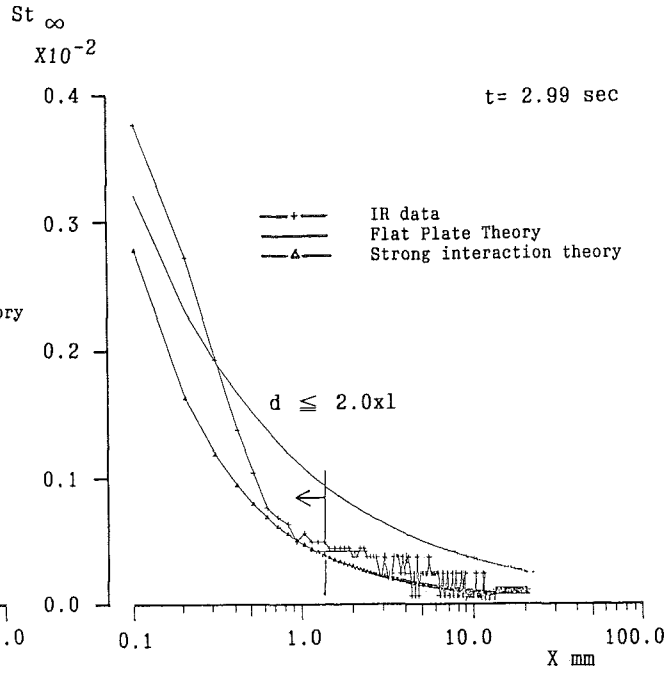

Fig.8b) Heat transfer distribution along centerline of flat plate
(M= 7.1, α = 0°, t= 2.99 sec)

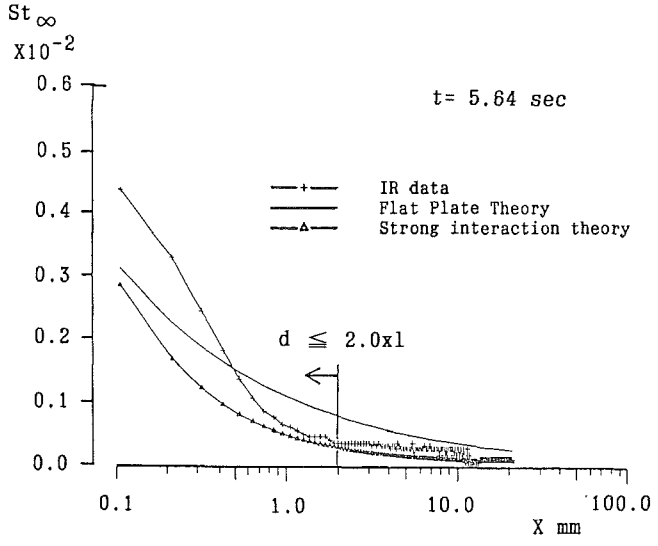

Fig.8c) Heat transfer distribution along centerline of flat plate
(M= 7.1, α = 0°, t= 5.64 sec)

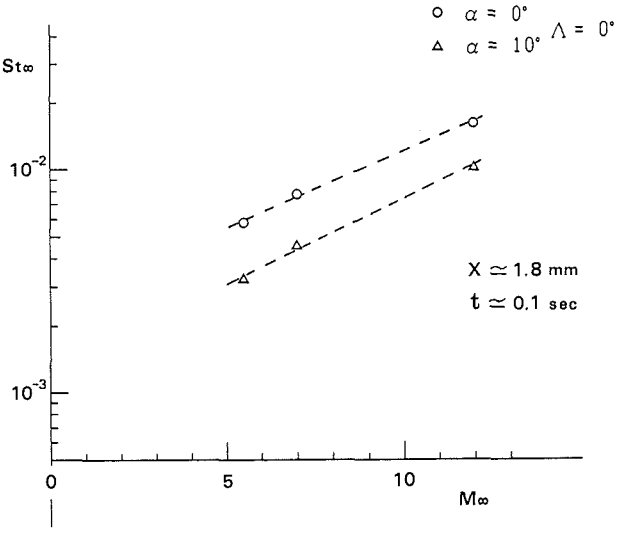

Fig.9 Heat transfer rate at leading edge region for flat plate
(M= 7.1, α = 0°)

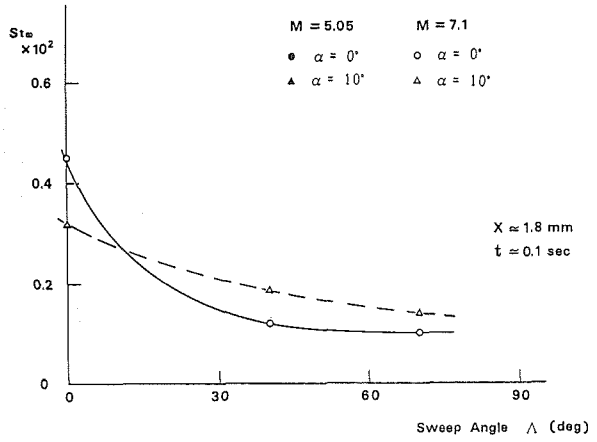

Fig.10 Effect of sweep angle on heat transfer at leading edge region

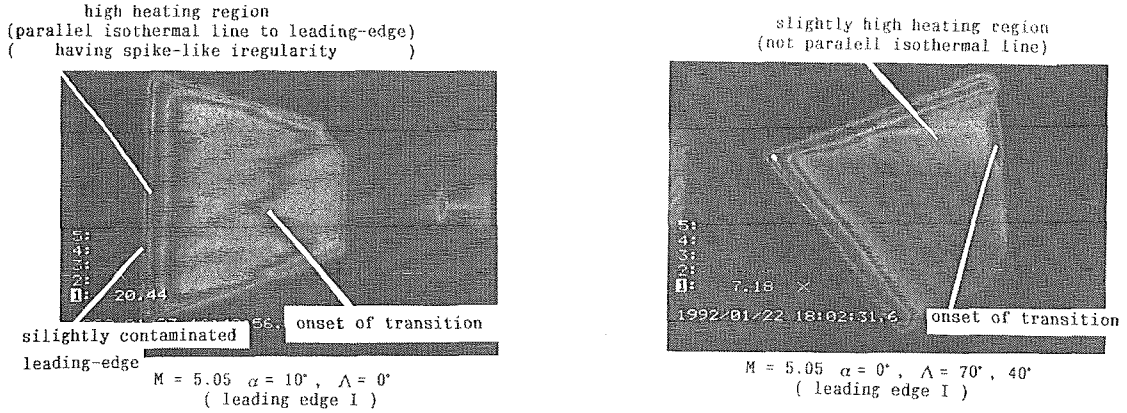

Fig.11a) Observation of boundary layer transition by IR thermographic images.
(M = 5.05, Type I leading edge)

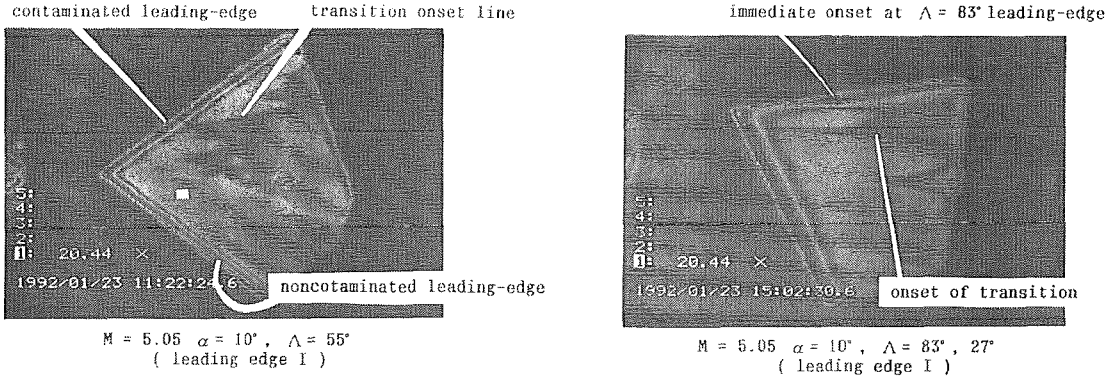

Fig.11b) Observation of boundary layer transition by IR thermographic images.
(M = 5.05, Type I leading edge)

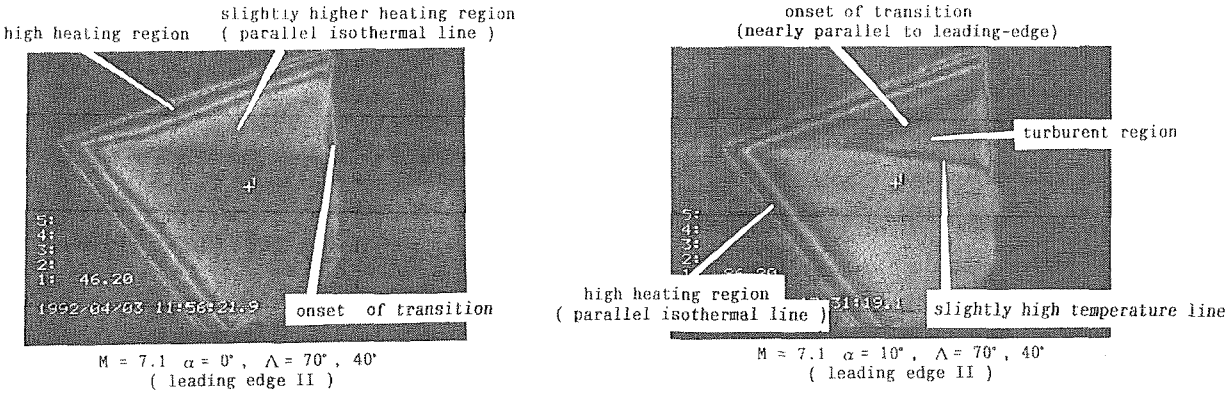

Fig.11c) Observation of boundary layer transition by IR thermographic images.
(M = 7.10, Type II leading edge)

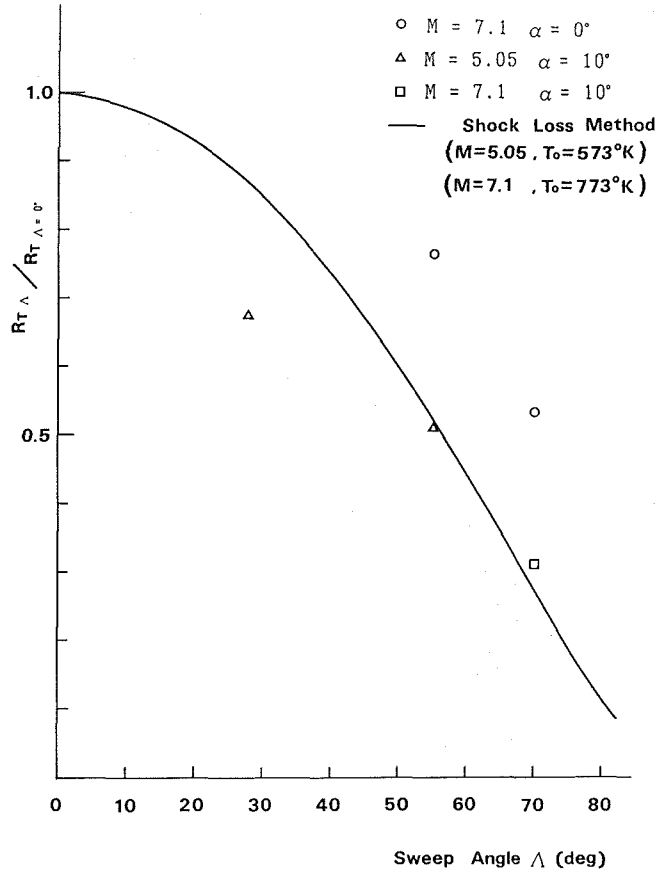

Fig.12 Effect of sweep angle on onset of transition on flat plate model